

Optical clearing assisted confocal microscopy of ex vivo transgenic mouse skin



Eunjoo Song^{a,1}, YoonJoon Ahn^{b,1}, Jinhyo Ahn^a, Soyeon Ahn^a, Changhwan Kim^c, Sanghoon Choi^b, Richard Martin Boutilier^b, Yongjoong Lee^b, Pilhan Kim^{a,*}, Ho Lee^{b,*}

^a Graduate School of Nanoscience and Technology, Korea Advanced Institute of Science and Technology (KAIST), Daehak-ro 291, Yuseong-gu, Daejeon 305-701, South Korea

^b School of Mechanical Engineering, Kyungpook National University, Sangyeok 3-dong, Buk-gu, Daegu, South Korea

^c School of Mechanical Design & Manufacturing, Busan Institute of Science and Technology, Sirang-ro 132beon-gil, Buk-Gu, Busan, Korea

ARTICLE INFO

Article history:

Received 19 January 2015

Received in revised form

26 March 2015

Accepted 31 March 2015

Available online 14 May 2015

Keywords:

Optical clearing

Transgenic mouse skin

Tissue clearing

ABSTRACT

We examined the optical clearing assisted confocal microscopy of the transgenic mouse skin. The pinna and dorsal skin were imaged with a confocal microscope after the application of glycerol and FocusClear. In case of the glycerol-treated pinna, the clearing was minimal due to the inefficient permeability. However, the imaging depth was improved when the pinna was treated with FocusClear. In case of dorsal skin, we were able to image deeply to the subcutaneous connective tissue with both agents. Various skin structures such as the vessel, epithelium cells, cartilage, dermal cells, and hair follicles were clearly imaged.

© 2015 Published by Elsevier Ltd.

1. Introduction

Most tissues are highly turbid media through which light is diffused by various scatterers including cell nuclei, organelles, membranes and extracellular matrix fibers. This scattering has been considered as one of the major factors that limits the imaging depth and contrast of most optical imaging modalities such as wide-field microscopy, confocal, nonlinear microscopy, and optical coherence-based tomography. The light scattering hinders both the light delivery to the sample and the detection of signals from the sample. Since the optical clearing assisted imaging has been used to study the human sclera in 1990s [1], numerous optical clearing agents (OCA) have been employed to improve the imaging depth and contrast of light-based imaging of cells and tissues [2]. The underlying mechanism of the optical clearing technique at the cellular and tissue levels has been investigated by many groups and it is generally accepted that the optical clearing is associated with the reduction of light scattering inside the tissue. Reduced scattering is mainly attributed to the dehydration, collagen dissociation, and the refractive index-matching between the light scatterers and the surrounding fluid [2–9]. In brief, the administration of the OCA into a tissue prompts the dehydration of the tissue because of the hyperosmosis of the agent. The OCA-induced concentration gradient

leads to the efflux of the water out of the tissue and the diffusion of the clearing agents into the cells and interstitial spaces. The replacement of water with the OCA results in the refractive index matching at the interface of the scatterers. This is because the refractive indices of the OCA agents closely match those of scatterers, compared with the refractive index of interstitial liquid [10]. The matched index reduces the scattering inside the tissue and the clarity of the tissue enhances. In addition to the refractive index-matching, the physical shrinkage of tissue followed by the dehydration and the dissociation of the collagen are also known to attribute to the reduction of light scattering.

Among various tissue types, the skin has been one of the most popularly examined tissues for the OCA-assisted imaging techniques. Optical clearing has been successfully used to enhance the penetration depth of the optical coherence tomography-based skin imaging [6,11]. Recently, the applications of optical clearing agents to the skin have been reported for the non-linear microscopic imaging methods including second harmonic microscopy, CARS microscopy and two-photon microscopy [12,13]. The feasibility of OCA-assisted Fourier transform infrared spectroscopic skin imaging has been tested as well [14]. In order to enhance the transdermal delivery of the OCA into the skin, several schemes including the micro-needle induced puncture, peeling of the stratum corneum using sandpaper, fractional laser induced microscopic ablation, and chemical enhancers have been proposed to overcome the epidermal barrier [15–21]. In spite of extensive studies on the OCA-assisted imaging of skin, OCA-assisted confocal skin imaging of a mouse model is lack of reporting,

* Corresponding authors.

E-mail addresses: pilhan.kim@kaist.ac.kr (P. Kim), hlee@knu.ac.kr (H. Lee).

¹ Contributed equally to this work.

especially for a transgenic mouse. There is a growing interest in confocal imaging of the skin of a genetically engineered mouse expressing fluorescent proteins to answer numerous biological questions related to the immune response, stem cell, gene therapy, and oncology [22–24]. It is essential to have comprehensive morphological information about the transgenic mouse skin to answer the dynamic cellular response in the field of immunology, oncology, and stem cells.

In this study, we investigated the optical clearing-assisted skin images of a transgenic mouse model using confocal microscopy. The transgenic mouse with two endogenous fluorescence proteins in cell nuclei and cytoskeletons was employed as an animal model to investigate the confocal-based morphological images of skin following the application of optical clearing agents. We have used two distinct optical clearing agents to test the feasibility of the optical clearing technique to the transgenic mouse skin. A home-built laser scanning confocal microscope was used to observe the morphological changes of the transgenic mouse skin following the application of the optical clearing agents. The images from the OCA-applied group and the control group were compared and the optimal optical clearing conditions were discussed.

2. Animals, materials and methods

The optically sectioned fluorescence images of the transgenic mouse pinna (the ear of the mouse) were acquired with a home-built confocal laser scanning microscopy which is operating for three fluorescence channels at 30 frames per second. The details on the microscopy are described in the previous publications [26]. In short, the home-built CLSM is based on the confocal detection utilizing two diode-pumped solid-state (DPSS) lasers and two photomultiplier tubes (PMT) with 100 μm pinholes. Two DPSS lasers with the wavelengths of 488 nm and 561 nm were employed to excite the green fluorescence protein (GFP) and the red fluorescence protein (RFP), respectively. A water immersion objective lens from Olympus with the numerical aperture of 0.6 and the magnification of 40 \times was used. The working distance of the objective lens is 170 μm and the field of view was set to 400 μm by 400 μm . In order to compare the signal intensity quantitatively, the excitation laser power and the amplification gain of PMT were set identical for different clearing conditions and application time of OCA.

The axial resolution of the CLSM can be defined as the axial position at which the detected intensity drops to the half the value on the focal plane. The measured axial resolution was about 7 μm : i.e. the CLSM can optically section the image planes every 7 μm . The analog signals from the PMTs were fed into the frame grabber along with the video synchronization signals. The digitally converted signals from the 10-bit frame grabber were used to acquire the snapshot images and movie streams with a Visual Basic-based custom written software.

Skin imaging of confocal microscopy was performed using a transgenic mouse model which co-expresses the green fluorescence protein (GFP) and the red fluorescence protein (DsRed). The dual-fluorescence protein expressing mouse model was produced by crossing two strains of mice that express GFP or DsRed. The first strain expresses H2B-EGFP fusion protein with coding sequence of histone 1 H2bb followed by enhanced GFP (B6.Cg-Tg(HIST1H2BB/EGFP) 1 Pa/J, Jackson Laboratory, USA). The second strain expresses red fluorescence protein variant DsRed under the control of the chicken beta actin promoter. Since the GFP was bound with the histone protein in nucleosomes and chromatin, it fluorescently labels the nucleus of all phenotype cells. In case of the DsRed, it is controlled by the promoter of actin, a major component of the microfilaments in the cytoskeleton of cells, which makes all tissues and cells fluoresce red. The double labeling of the nucleus and the cytoskeleton is a well-established standard for the visualization of

individual cells and their interactions with the microenvironment in tissues. Twelve weeks old Actin-GFP and DsRed mice were used for the current study. All mice were bred in specific pathogen-free animal facility at KAIST and fed with ad libitum access to standard diet (PMI Lab diet) and water. Animals were euthanized by the injection of anesthetics right before excision of tissue sample. Animal care and experimental procedures were performed under the approval from the Animal Care Committee of KAIST (approval No. KA2013-11).

The skin of the pinna from a transgenic mouse was used as the primary imaging spot in the current study. The pinna was chosen as the primary sample because both sides of the pinna are covered with the epidermis that serves as the skin barrier for the transdermal delivery of active agents. The entire pinna was removed from a mouse and dissected into multiple sheets with the dimension of approximately 10 \times 5 mm² (4 ear pinna out of 2 mice). We used the dorsal skin (the skin on the back of the mouse) as a secondary imaging sample. The dorsal tissue was chosen for imaging because the outer side of the dorsal tissue is covered with the epidermis and dermis, while the inner side of the dorsal tissue is covered with the subcutaneous layer unprotected by the epidermal barrier. The dorsal skin was removed from live mice and dissected into sheets with a dimension of 5 \times 5 mm². The freshly excised samples were immersed in the OCA for clearing. The samples treated and untreated (control sample) with the clearing agent were placed on an automated translation stage for confocal imaging, and the automated stage allowed the sequential *en-face* images stacking at multiple depths from the surface. Two detection channels were employed to image red fluorescence and green fluorescence independently.

Two different optical clearing agents were employed in the current study: glycerol and FocusClear™ (CelExplorer, Hsinchu, Taiwan). Glycerol was chosen as it is one of the most popularly investigated optical clearing agents along with other alcohol such as PEG (polyethylene glycol), butanediol, and propanediol [2]. Glycerol is a water-soluble alcohol and its refractive index is 1.47 [25]. Because of its bio-compatibility, glycerol has been applied for in vivo tissues and the potential side effects such as local cell necrosis and vessel hemostasis have been reported. It has been also reported that the different concentrations and application time are necessary to achieve the optimal tissue clearing for various tissue types in vivo and in vitro. In the current study, the volumetric concentration of glycerol was 70% in PBS solution. The second optical clearing agent employed is a dimethyl sulfoxide (DMSO) based commercial optical clearing agent named FocusClear™. Its secondary ingredients include diatrizoate acid, ethylenediamineteraacetic acid, glucamine, B-nicotinamide adenine dinucleotide phosphate, sodium diatrizoate and a derivative of polyoxyalkalene in a suitable aqueous solution [27]. FocusClear was first applied for the imaging of a neural circuit of an insect brain, and its application has been expanded for various tissue types including intestinal microvasculature and kidney [27–29]. The standard application protocol for the optical clearing agents is followed. The OCA was stored in a refrigerator at 4 °C prior to the usage. The skin samples were dissected from live transgenic mice, and they are immersed in two different types of tissue clearing solutions for 30 min, one hour, and three hours. For the control group, the samples were immersed in PBS solution for 30 min.

3. Results

3.1. Anatomy of murine pinna

A simple illustration of the murine ear skin is illustrated in Fig. 1 based on literature surveys. The thickness of the pinna is

about one millimeter, and it consists of three major layers: epidermis, dermis and articular cartilage. The cartilage is located in the middle of the pinna. The dermis and the epidermis are placed symmetrically on both sides of the cartilage. The non-viable cells with no nucleus form the top epidermal layer (called “stratum corneum”) is responsible for the physical epidermal barrier functions. The stratum corneum is followed by a viable epidermal cell layer in which epidermal cells are densely packed and distinguishable by their depth from the surface. The size of epidermal cells decreases and the density of cells increases with the depth from the surface. The deepest layer of the epidermis is a continuous cell layer called “papillary basal layer”, and the papillary basal layer constitutes the border between the epidermis and the dermis. The dermis is located under the basal layer, and it plays an important role as the frontline gate keeper of body along with the epidermis. In the dermis, there exist various features including the extracellular matrix, immune cells, lymphatic/blood vessels, and

hair follicles. The structural integrity of the dermis is maintained by the extracellular matrix (collagen and elastin fibers), and the fibroblasts being a phenotype of dermal cells responsible for the production of the extracellular matrix. The cellular immune response of skin is controlled by resident immune cells (mast cells and dendritic cells) and migrating cells trafficking through the lymphatic and blood vessels. In addition to the hair shaft, a hair follicle consists of various features including the sebaceous gland, the arrector pili muscle, root sheath and hair matrix. The hair growth takes place inside the hair matrix which consists of the germinal epithelium cells and melanocytes. As it grows, the hair shaft is surrounded by the root sheath, which is the collection of epidermal cells differentiated in the hair matrix. The sebaceous gland produces the oil for the lubrication and waterproofing of hair follicles, and arrector pili muscle makes the hair stand up. One of the most interesting morphological features of the murine pinna is the articular cartilage. The cartilage symmetrically divides the pinna into two sides and it is responsible for the shape of the pinna.

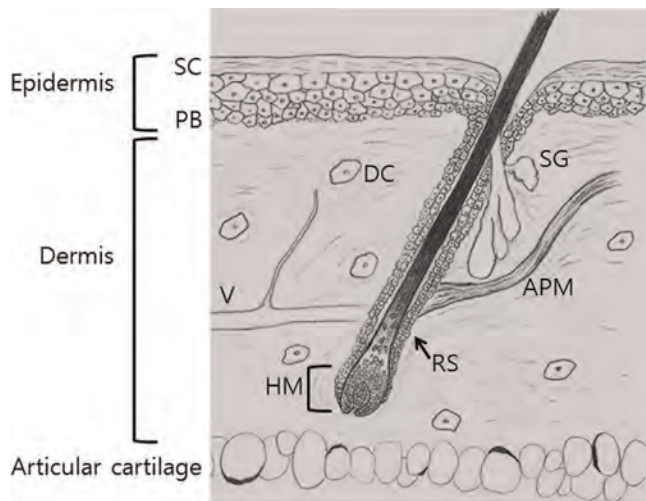


Fig. 1. Anatomy of murine ear pinna. The murine ear consists of three major layers which are epidermis, dermis and articular cartilage. SC: stratum corneum, PB: papillary basal, V: vessel, SB: sebaceous gland, APM: arrector pili muscle, RS: root sheath, HM: hair matrix, and DC: dermal cell.

3.2. Photography of skin clearing

The degree of transparency change of the OCA-treated pinna was evaluated by placing the sample on top of an imaging target with grids (Fig. 2).

The digital photographs of the pinna were taken before and after the treatment with the OCA. In case of the control and glycerol-treated samples, the transparency of the samples was not altered significantly so that the underlying grid of the target was not visible after three hours of treatment (Fig. 2(a) and (b)). However, the transparency of FocusClear-treated sample became enhanced, and the underlying grid was visible after three hours of treatment (Fig. 2(c)).

3.3. B-scan and 3D rendered confocal images of transgenic mouse skin of pinna

The *en-face* image stacks of the control and OCA-treated groups of the pinna skin were taken using a z-axis translation stage every 3 μm in the direction of depth from the surface. The power of excitation laser and the amplification factor for the

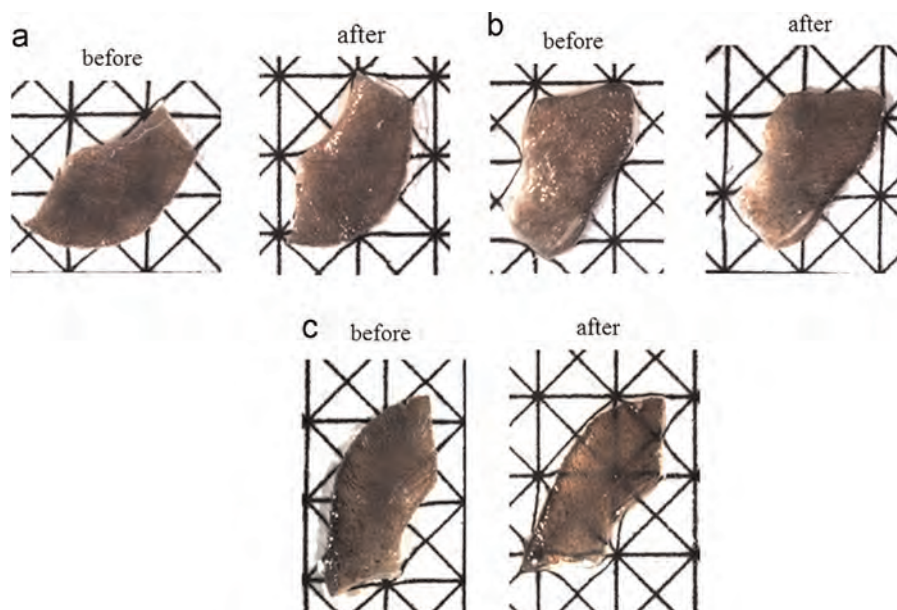


Fig. 2. Transparency change of ear pinna before and after the treatment with clearing agents (a) control, before and after three hours treatment in PBS, (b) glycerol treated group, before and three hours treatment and (c) FocusClear treated group, before and three hours treatment. Each main vertex of the grid is 0.5 cm apart.

photomultiplier tubes were adjusted identically for all clearing conditions. Four spots were imaged for each clearing conditions. In order to assess the imaging depth for different OCA conditions, we compared the typical B-scan images (2D cross-sectional view orthogonal to the *en-face* image) which was reconstructed from

acquired *en-face* image stacks with a rendering software (Image J, National Institutes of Health, USA (Fig. 3)).

The images are sorted by the clearing conditions (control group (a), glycerol-treated group (b–d), FocusClear-treated group (e–g)), and the treatment time (30 min, one hour, and three hours).

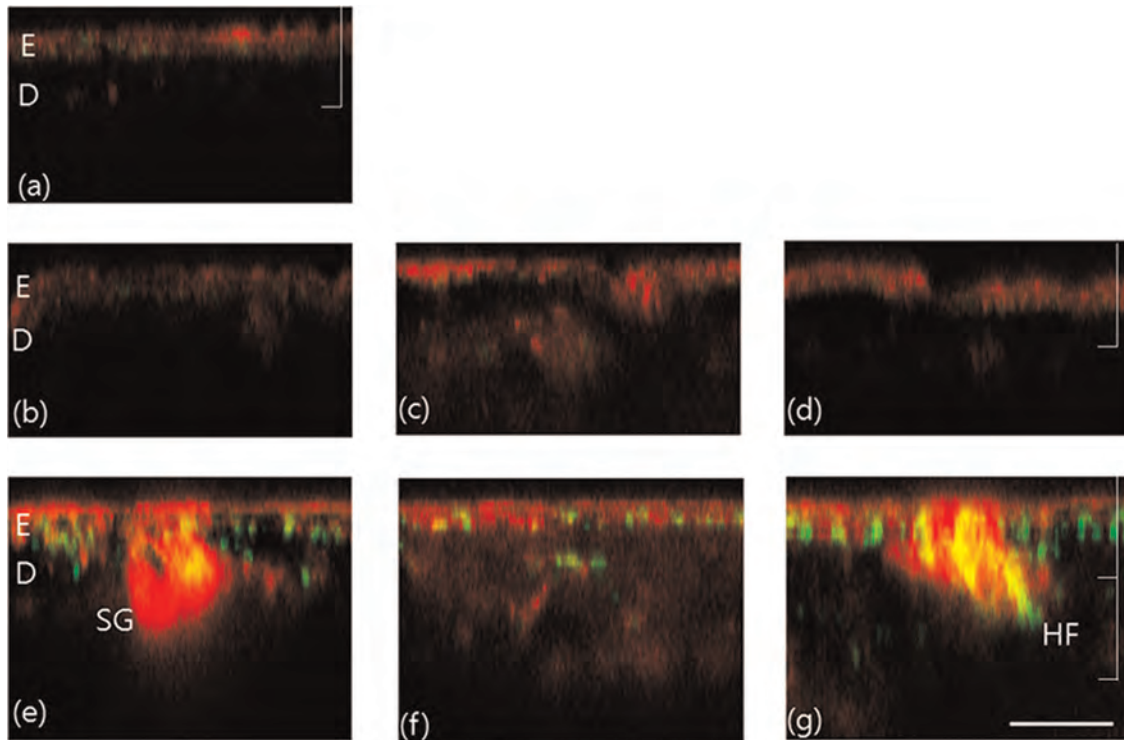


Fig. 3. B-scan confocal image of transgenic mouse skin. (a) Control, (b) glycerol, 30 min, (c) glycerol, one hour, (d) glycerol, three hours, (e) FocusClear, 30 min, (f) FocusClear, one hour and (g) FocusClear, three hours. E: epidermis, D: dermis, SG: sebaceous gland, and HG: hair follicle. Scale bar is 50 μm . Each vertical tic represents 50 μm . (For interpretation of the references to color in this figure, the reader is referred to the web version of this article.)

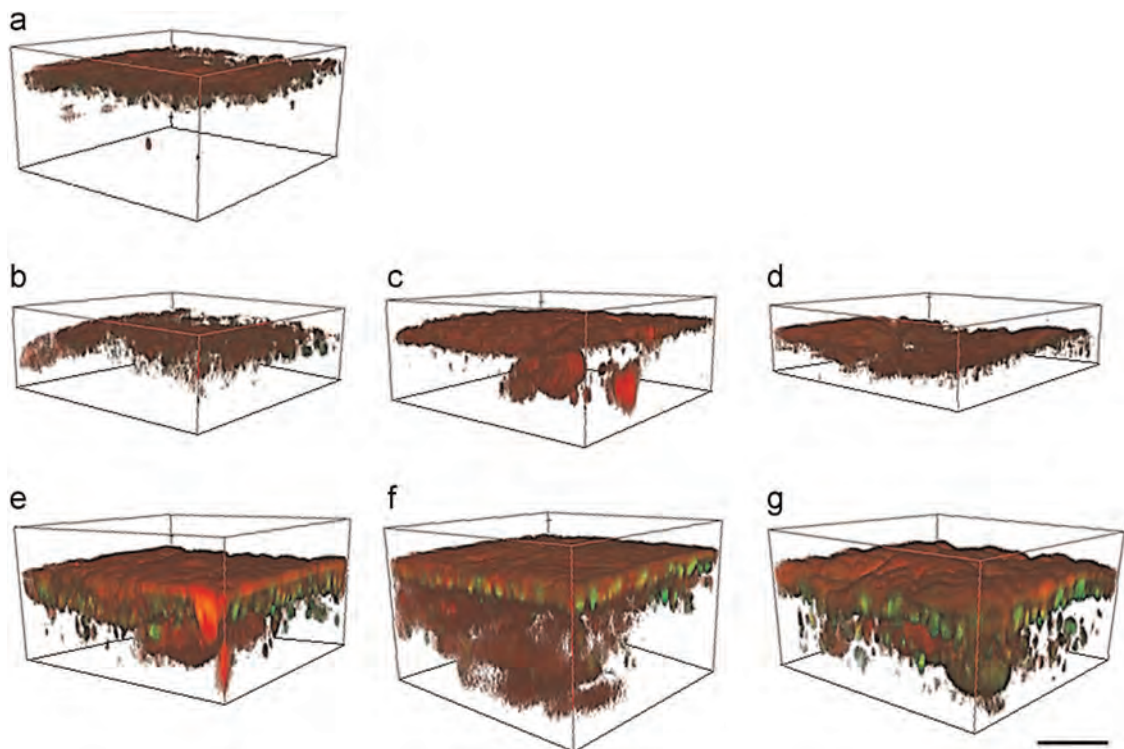


Fig. 4. 3D confocal images of transgenic mouse skin. (a) Control, (b) glycerol, 30 min, (c) glycerol, one hour, (d) glycerol, three hours, (e) FocusClear, 30 min, (f) FocusClear, one hour and (g) FocusClear, three hours. Scale bar is 50 μm . (For interpretation of the references to color in this figure legend, the reader is referred to the web version of this article.)

Regardless of the clearing conditions, the epidermal layer composed of dense epidermal cells distinguished itself from the dermal layer primarily composed of the extracellular fibrous network with less densely populated dermal cells. The epidermal layer (E) appears as the bright top layer with a thickness of approximately 20 μm , while the dermal layer (D) is located beneath the epidermis with a few distinct dermal structures. One of the most highlighted dermal structures is the hair follicle (HF) which appears as a mixture of red and green fluorescence. The sebaceous gland (SG) of the hair follicle is the primary source of red fluorescence, and the cell nucleus near the hair shaft presents strong green fluorescence.

While B-scan images of various clearing conditions show common features, there exist noticeable differences depending on the clearing conditions. The confocal microscope was able to image primarily the upmost epidermis layers for the control group immersed in PBS without OCA treatment. In case of the glycerol-treated sample, sporadic fluorescence originating from various dermal structures was observed beneath the epidermis. However, the imaging depth of glycerol-treated sample is comparable with that of the control group. In contrast to the control and glycerol-treated samples, the imaging depth and signal brightness were enhanced for samples treated with FocusClear. Particularly, the

imaging depth was enhanced up to 150 μm for samples treated with FocusClear for one or three hours. The epidermal layers and hair follicles from the FocusClear-treated samples appear brighter than those in the control and the glycerol-treated samples.

The 3D reconstruction was performed using the stack of *en-face* images, and the perspective views of two-color 3D rendered images of the transgenic mouse pinna skin were presented for various clearing conditions (Fig. 4). The overall integrity such as the surface wrinkle, basal border and imaging depth were outlined with red fluorescence, while the green channel depicts the three-dimensional distribution of cell nuclei. Three-dimensional morphology of the dermis was also highlighted in the rendered images. In particular, dermal features such as the hair follicle, extracellular matrix, and randomly distributed cells were clearly illustrated in the FocusClear-treated samples.

3.4. *En-face* images of murine ear pinna

Various skin features of the transgenic mouse pinna can be presented with the *en-face* image mode. The *en-face* images for different clearing conditions are compared in Fig. 5.

The presented *en-face* images are taken after 30 min for the control, one hour for glycerol-treated, one and three hours for the

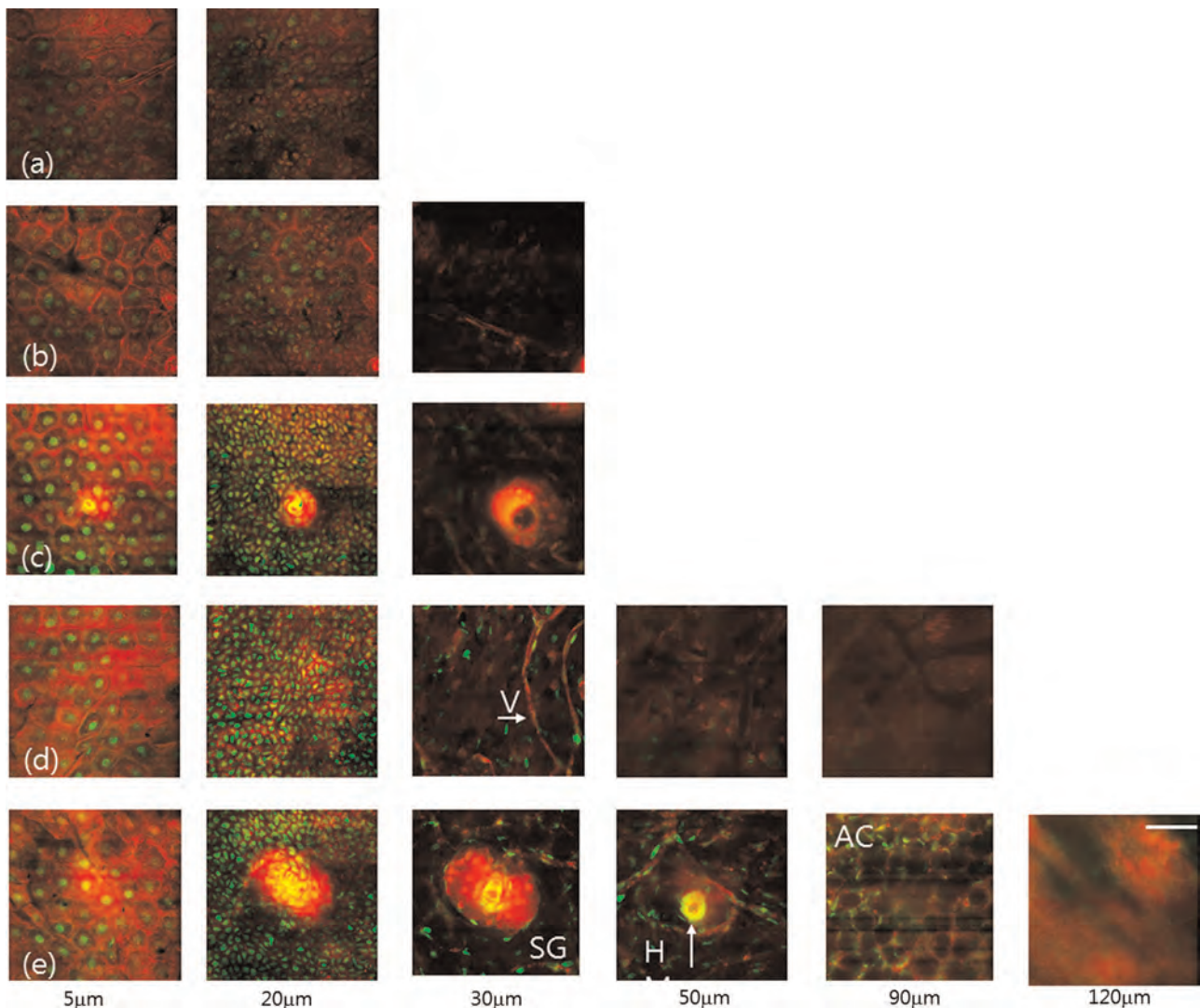


Fig. 5. *En-face* images of murine ear pinna. (a) Control, (b) glycerol, one hour, (c) FocusClear, 30 min, (d) FocusClear, one hour and (e) FocusClear, three hours. V: vessel, SG: sebaceous gland, HM: hair matrix, and AC: articular cartilage. Scale bar is 50 μm . (For interpretation of the references to color in this figure legend, the reader is referred to the web version of this article.)

FocusClear-treated samples. The *en-face* images were taken from the surface of the skin, 5 μm , 20 μm , 30 μm , 50 μm , 90 μm , and 120 μm deep from the surface. The epidermal cell layers were clearly observed for all three conditions. The nuclei of epidermal cells express bright GFP signals while the cytoplasm and cell membrane are distinguished by red fluorescence. The size of nuclei for epidermal cells varies with the depth, and the tightly packed basal cells indicate the papillary junction between the epidermis and the dermis. It should be noted that the brightness of both green and red fluorescence in the FocusClear-treated samples are much brighter than the control and the glycerol-treated samples.

As in the B-scan image, the deepest imaging was possible for the FocusClear-treated samples, and various structures in the dermis such as hair follicles, vessels (V) and dermal cells were visualized. The epithelium cells express bright green fluorescence, and the sebaceous gland (SG) is mainly presenting RPF. The nucleus of epidermal origin in the sebaceous gland was also visualized. The epidermal cells in the hair matrix (HM) were observed with bright green signals and distributed circularly around the hair shaft. Along with the hair follicles, we were able to image the extracellular fibrous matrix expressing DsRed, less densely populated dermal cells with GFP (Fig. 5(d)), and the vessels with elongated endothelium cells. In case of the FocusClear-treated samples, the uniform articular cartilage (AC) with an approximate diameter of 20 μm was observed near the depth of 100 μm (Fig. 5(e)). The circular porous structures with a red boundary were imaged, and few micron-size nuclei of chondrocytes exist at the edge of the cartilage boundary. It should be noted that we were able to image the opposite dermal layer (the dermal layer located below the articular cartilage) due to the enhanced imaging depth by the optical clearing agent. Beyond the cartilage, the hair bulb and extracellular matrix of the opposite dermal layer were observed as well

3.5. B-scan and 3D rendered confocal images of the dorsal skin of the transgenic mouse

The dorsal skin was employed as a secondary imaging target in order to examine the effects of the epidermis for the transdermal delivery of clearing agents. In contrast to the pinna which is covered by the skin on both sides, the dorsal tissue has the skin on one side and the other side is covered by subcutaneous components. Excised dorsal tissues were immersed in the clearing agents for one and three hours prior to confocal imaging. Optimal laser and PMT parameters were pre-determined for dorsal skin imaging, and the sequential *en-face* images were taken at different depths from the surface. Two spots were imaged for each clearing condition. In order to assess the imaging depth, we compared the B-scan images and 3D rendered images for various clearing conditions (Fig. 6).

In contrast to the pinna, noticeable clearing effects were observed for both glycerol and FocusClear treated samples. While the confocal microscope was able to image approximately 100 μm below the surface for the control sample, the imaging depth increased up to 300 μm with stronger fluorescence from the hair follicle and subcutaneous connective fibrous tissues for the glycerol and FocusClear-treated samples.

4. Discussion

Skin is one of the most popularly imaged tissues with optical imaging modalities including confocal microscopy, nonlinear microscopy and optical coherence tomography. In vitro and in vivo imaging of animal model skin facilitates to answer various questions in the fields of immunology, oncology, and stem cells [22–24]. A commercial confocal microscope is also available for the microscopic observation of human skin to monitor the skin aging, melanoma, and transdermal delivery [30]. Despite confocal microscopy has been used successfully in numerous applications, the imaging

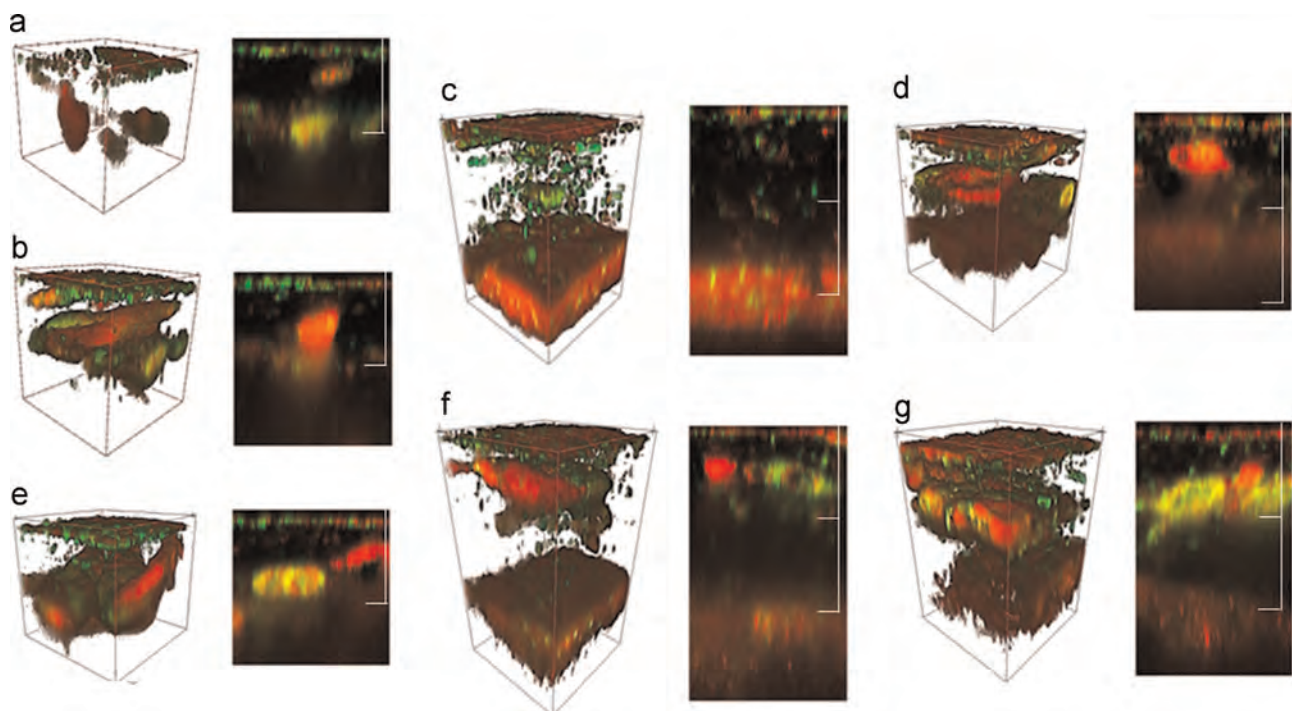


Fig. 6. 3D and B scan confocal images of dorsal skin of transgenic mouse. (a) Control, (b) glycerol, 30 min, (c) glycerol, one hour, (d) glycerol, three hours, (e) FocusClear, 30 min, (f) FocusClear, one hour and (g) FocusClear, three hours. Scale bar is 100 μm . Each vertical tic represents 100 μm .

depth of confocal-based skin observation is limited to approximately 100 μm from the surface, and the image contrast deteriorates dramatically with the depth. The primary origin of these constraints is associated with the scattering nature of turbid skin. Various optical clearing agents have been applied for skin imaging to enhance the contrast and imaging depth by means of the scattering reduction in optical coherence tomography, two photon microscopy, and CARS microscopy.

In the current study, we examined the efficacy of the optical clearing technology for the confocal imaging of the transgenic mouse skin. We employed two distinct optical clearing agents (glycerol and FocusClear). We selected the pinna of a mouse as a primary imaging target since both sides of the pinna are covered with the epidermis which works as the natural skin barrier. The dorsal tissue was selected as a secondary imaging target since the dorsal tissue has the skin only on one side. The other side of the dorsal tissue is covered by subcutaneous components that provide no barrier function.

When the pinna was treated with glycerol over the span of three hours, a localized clearing effect was observed. However, the overall enhancement in the imaging depth and contrast was not significant. In contrast to the pinna, we observed a noticeable optical clearing when the dorsal skin is treated with glycerol. Compared to the control group, the imaging depth of the glycerol-treated dorsal skin became enhanced by a factor of two. The minimal clearing effect of glycerol on the pinna can be attributed to the inefficient diffusion of glycerol through the skin barrier. It has been reported that the transdermal delivery of glycerol is very restricted when it is applied topically on skins. Because of this, the subcutaneous injection of glycerol and physical/chemical destruction of the epidermal barrier were suggested in order to enhance the transdermal delivery of glycerol into the skin [15–21]. In order to achieve an enhanced imaging depth and contrast with glycerol, additional steps for the effective transdermal delivery of glycerol are suggested.

The imaging depth and contrast were improved when the pinna and dorsal skin were immersed in the FocusClear solution for 30 min to three hours. The FocusClear-induced clearing contributed to the detection of brighter fluorescence signals from the sample. This resulted in high contrast images of skin structures such as the capillary vessels with epithelium cells, articular cartilage, dermal cells and hair follicles. It is worth mentioning that the opposite dermal site beyond the articular cartilage was also observed in the FocusClear-treated pinna. The FocusClear induced clearing on the pinna suggests that FocusClear effectively overcame the epidermal skin barrier on both sides of the pinna and diffused into the dermal region successfully. The enhanced permeability of FocusClear can be attributed to DMSO which is one of the active components. DMSO, an organic solvent, has been utilized as a permeability enhancer for the skin by inducing microscopic pores on the cell membranes [14,31].

In a direct comparison of Glycerol and FocusClear™ as OCAs, both performed nearly as well at optical clearing relative to imaging depth when the epidermal layer was not an obstacle, as was the case for the samples of dorsal skin. This is likely due to their similar index of refractions; an extrapolated value of ~ 1.43 [32] for a 30/70% PBS and glycerol solution and 1.46 for FocusClear solution [10]. However, when the epidermal layer is encountered, glycerol showed very little penetration whereas FocusClear™ maintains a similar depth of penetration as when the epidermal layer was absent. The main ingredient of FocusClear™, DMSO, is thought to have a high capability of penetrating cellular membranes [33]. Hypothetically, this would allow it to tunnel through adjacent cells. In contrast, glycerol does not penetrate cell membranes at room temperatures [33] even within extended periods of time [14]. Furthermore, glycerol's high hydrophilicity may be

responsible for impeding its passage through the confined intercellular space of the densely packed epidermal layer cells [14].

It should be noted that the hair follicle is one of the most outstanding features in the dermis when the transgenic mouse skin is imaged with confocal microscopy using the optical clearing technology. Most components of the hair follicle such as the shaft, sebaceous gland, epidermal cell near the hair matrix present strong fluorescence. The overall structure of the hair follicle was more clearly imaged compared to the surrounding dermal region. A strong signal from the hair follicle can be attributed to two factors. The first is the densely populated epithelial cells in the hair follicle, and the second is the easy access for the clearing agent into the hair follicle. The hair follicle is epithelial in nature, and it is a part of the epidermis. The epithelium stem cell in the hair matrix is responsible for the hair regrowth and recycling. The hair matrix is known as one of the most active germinal sites in a human body, so numerous epithelial cells are located in the matrix, inner and outer sheaths of hair. These densely populated epithelial cells make the hair follicles appear brighter than the surrounding dermis region. The drug transport through the hair follicle duct is one of the major pathways for the transdermal delivery of active chemical agents into the skin. The facilitated transport of the clearing agent through the hair follicle could lead to the enhanced optical clearing of epithelial cells in the hair follicle [34]. The results of the current study suggest that confocal imaging of the skin treated with an optical clearing agent can be applied to various hair follicle-related studies such as the hair growth, hair transplant, and tissue engineering involving epithelium stem cells.

5. Conclusion

We have successfully applied optical clearing-assisted confocal microscopy to image the ex vivo transgenic mouse skin. The pinna and dorsal skin of transgenic mice with H2B GFP and actin DsRed was imaged with a home-built confocal microscope after the application of glycerol and FocusClear to the samples. In case of the glycerol-treated pinna, the clearing effect was not significant compared to the control sample. The minimal optical clearing by glycerol on the pinna was attributed to the inefficient diffusion through the skin barrier. In case of the FocusClear-treated pinna and dorsal skin, the imaging depth and signal intensity improved. The entire epidermal and dermal layers on one side of the pinna and subcutaneous structures of dorsal tissue could be imaged, and various skin structures such as the capillary vessel with epithelium cells, articular cartilage, dermal cells and hair follicles were clearly imaged. These observations suggest that FocusClear can overcome the epidermal skin barrier and effectively diffuse into the dermal layer because of the enhanced permeability by DMSO. This region is of particular usefulness for ex vivo studies intending to image structures which remain morphologically unchanged by the clearing process. In addition, by controlling the immersion time within the FocusClear™ solution, it should be possible to control the depth of optically cleared tissue such that important biological processes remain intact at a level just below the depth of the cleared region. Confocal microscopy can then be used to image these deep tissue processes which are located below the optically cleared top layer. Thus, the use of FocusClear™ should prove also to be a valuable tool for in vivo studies. More specifically, the results of the current study suggest that the optical clearing assisted confocal microscopy can be applied to various studies involving the hair growth, the epithelium stem cell behavior in a niche, and the immune cell trafficking in skin.

Acknowledgments

This study was supported by a Grant of the Korean Health Technology R&D Project, Ministry of Health & Welfare, Republic of Korea (Grant No. HN12C0063). This study was supported by the Human Resource Training Project for Regional Innovation MOE and NRF-2014H1C1A1066748.

References

- [1] Tuchin VV, Maksimova IL, Zimnyakov DA, Kon IL, Mavlutov AK, Mishin AA. Light propagation in tissue with controlled optical properties. *J Biomed Opt* 1997;2:401–17.
- [2] Zhu D, Larin KV, Luo Q, Tuchin VV. Recent progress in tissue optical clearing. *Laser Photon Rev* 2013;7:732–57.
- [3] Chung K, Wallace J, Kim SY, Kalyanasundaram S, Andalman AS, Davidson TJ, et al. Structural and molecular interrogation of intact biological systems. *Nature* 2013;497:332–7.
- [4] Tuchin VV. Optical clearing of tissues and blood using the immersion method. *J Phys D: Appl Phys* 2005;38:2497–518.
- [5] Vargas G, Chan EK, Barton JK, Rylander III HG, Welch AJ. Use of an agent to reduce scattering in skin. *Lasers Surg Med* 1999;24:133–41.
- [6] Khan MH, Choi B, Chess S, Kelly KM. Optical clearing of in vivo human skin: implication for light-based diagnostic imaging and therapeutics. *Lasers Surg Med* 2004;34:83–5.
- [7] Hama H, Kurokawa H, Kawano H, Ando R, Shimogori T, Noda H, et al. Scale: a chemical approach for fluorescence imaging and reconstruction of transparent mouse brain. *Nat Neurosci* 2011;14:1481–8.
- [8] Meglinsky IV, Bashkatov AN, Genina EA, Churmakov DYU, Tuchin VV. The enhancement of confocal image of tissues at bulk optical immersion. *Laser Phys* 2003;13(1):65–9.
- [9] Smatham R, Phillips KG, Jacques SL. Assessment of optical clearing agents using reflectance-mode confocal scanning laser microscopy. *J Innov Opt Health Sci* 2010;3(3):183–8.
- [10] Genina EA, Bashkatov AN, Tuchin VV. Tissue optical immersion clearing. *Expert Rev Med Devices* 2010;7:725–847.
- [11] Proskurin SG, Meglinsky IV. Optical coherence tomography imaging depth enhancement by superficial skin optical clearing. *Laser Phys Lett* 2007;4:824.
- [12] Cicchi R, Sampson D, Massi D, Pavone F. Contrast and depth enhancement in two-photon microscopy of human skin ex vivo by use of optical clearing agents. *Opt Express* 2005;14:2337–44.
- [13] Zimmerley M, McClure RA, Choi B, Potma EO. Following dimethyl sulfoxide skin optical clearing dynamics with quantitative nonlinear multimodal microscopy. *Appl Opt* 2009;48:D79–87.
- [14] Jiang J, Boese M, Turner P, Wang RK. Penetration kinetics of dimethyl sulphoxide and glycerol in dynamic optical clearing of porcine skin tissue studied by Fourier transform infrared spectroscopic imaging. *J Biomed Opt* 2008;13:021105.
- [15] Stumpp O, Chen B, Welch B. Using sandpaper for noninvasive transepidermal optical skin clearing agent delivery. *J Biomed Opt* 2006;11:04118.
- [16] Yoon J, San T, Choi EH, Nelson JS, Jung B. Enhancement of optical skin clearing efficacy using a microneedle roller. *J Biomed Opt* 2008;13:021103.
- [17] Yoon J, Park D, San T, Seo J, Nelson JS, Jung B. A physical method to enhance transdermal delivery of a tissue optical clearing agent: combination of microneedling and sonophoresis. *Lasers Surg Med* 2010;42:412–7.
- [18] Genina EA, Dolotoy LE, Bashkatov AN, Terentyuk GS, Maslyakova GN, Zubkina EA, et al. Fractional laser microablation of skin aimed at enhancing its permeability for nanoparticles. *Quantum Electron* 2011;41:396–401.
- [19] Genina EA, Bashkatov AN, Tuchin VV, Altshuler GB, Yaroslaysky IV. Possibility of increasing the efficiency of laser-induced tattoo removal by optical skin clearing. *Quantum Electron* 2008;38:580–7.
- [20] Jiang J, Wang RK. Comparing the synergistic effects of oleic acid and dimethyl sulfoxide as vehicles for optical clearing of skin tissue in vitro. *Phys Med Biol* 2004;49(23):5283–94.
- [21] Xu X, Zhu Q. Evaluation of skin optical clearing enhancement with Azone as penetration enhancer. *Opt Commun* 2007;279:223–8.
- [22] Ghigo G, Mondor I, Jorjue A, Nowak J, Wienert S, Zahner SP, et al. Multicolor fate mapping of Langerhans cell homeostasis. *J Exp Med* 2013;210:1657–64.
- [23] Blanpain C, Lowry WE, Geoghegan A, Polak L, Fuchs E. Self-renewal, multipotency, and the existence of two cell populations with an epithelial stem cell niche. *Cell* 2004;118:635–48.
- [24] Ra H, Emilio GG, Bryan RS, Sanjiv SG, Gordon SK, Olav S, et al. Assessing delivery and quantifying efficacy of small interfering ribonucleic acid therapeutic in the skin using a dual-axis confocal microscope. *J Biomed Opt* 2010;15(3):036027.
- [25] Veileux I, Spencer JA, Biss DA, Cote D, Lin CP. In vivo cell tracking with video rate multimodality laser scanning microscopy. *IEEE J Sel Top Quantum Electron* 2008;14(1):10–8.
- [26] Jungermann E. Glycerine: a key cosmetic ingredient. In: Jungermann Eric, Sonntag Norman OV, editors. *Physical properties of glycerine*. New York: Marcell Dekker, INC.; 1991. p. 113–56.
- [27] Ann SC. Aqueous tissue clearing solution. United States patent (16) patent N6; US 6,472,216 B1; 2002.
- [28] Yuan FY, Tang TSC. Optical clearing facilitates integrated 3D visualization of mouse ileal microstructure and vascular network with high definition. *Microvasc Res* 2010;80:512–21.
- [29] Hyink D. Three-dimensional imaging of fetal mouse kidneys. *Methods Mol Biol* 2012;886:87–93.
- [30] (<http://www.caliberid.com/product-overview.html>).
- [31] Karma S, Homan J, Stolanovicil C, Choi B, Innov J. Enhanced fluorescence imaging with DMSO-mediated optical clearing. *J Innov Opt Health Sci* 2010;3(3):153–8.
- [32] Leica Microsystems. Adaptation to the actual refractive index. *Confocal application letter resolution*. No. 17; 2004, p. 6.
- [33] McGann LE. Differing actions of penetrating and nonpenetrating cryoprotective agents. *Cryobiology* 1978;15:382–90.
- [34] Genina EA, Bashkatov AN, Sinichkin YuP, Kochubey VI, Lakodina NA, Altshuler GB, et al. In vitro and in vivo study of dye diffusion into the human skin and hair follicles. *J Biomed Opt* 2002;7:471–7.